Stokes and anti-Stokes resonant Raman scatterings from biased GaN/AlN heterostructure

Guibao Xu,[1] Suvranta K. Tripathy,[1] Xiaodong Mu,[1] Yujie J. Ding,[1,a)] Kejia Wang,[2] Yu Cao,[2] Debdeep Jena,[2] and Jacob B. Khurgin[3]
[1]*Department of Electrical and Computer Engineering, Lehigh University, Bethlehem, Pennsylvania 18015, USA*
[2]*Department of Electrical Engineering, University of Notre Dame, Notre Dame, Indiana 46556, USA*
[3]*Department of Electrical and Computer Engineering, Johns Hopkins University, Baltimore, Maryland 21218, USA*

(Received 8 June 2008; accepted 13 July 2008; published online 8 August 2008)

An electric field present in a GaN/AlN heterostructure can bring both the first-order and second-order Raman scattering processes into strong resonances. The resonant Stokes and anti-Stokes Raman scatterings result in the increase and decrease in nonequilibrium longitudinal-optical phonon temperatures, respectively. Moreover, the phonon temperature measured from the Raman scattering is increased with an applied electric field at a much higher rate than the lattice temperature due to the presence of field-induced nonequilibrium longitudinal-optical phonons. © *2008 American Institute of Physics*. [DOI: 10.1063/1.2967337]

Due to the Fröhlich interaction, it takes no more than 100 fs for an electron to emit one longitudinal-optical (LO) phonon in GaN.[1–3] In contrast, the time constant for the decay of the emitted LO phonons into transverse-optical and acoustic phonons[4] is 2.8 ps.[5] Even if GaN is pumped below its bandgap, such a constant was measured by us to be 4.2 ps. Since the LO phonons generated by electrons are accumulated, phonon occupancies are elevated,[6–8] i.e., the nonequilibrium or hot phonons are induced. Previously, the hot-phonon temperature and lifetime were estimated from a biased AlGaN/AlN channel based on microwave noise technique.[6] Among different techniques, Raman scattering may be one of the most direct techniques for investigating hot phonons based on the previous result.[7]

The accumulation of the hot phonons not only causes electron velocities to saturate but also leads to additional power dissipation,[8–11] and therefore, the corresponding electronic devices will deteriorate in time. Even though the GaN-based high-electron-mobility transistor (HEMT) may be the next-generation microwave power amplifiers with the possibilities of handling high powers as well as operating within a wide bandwidth,[12] hot phonons could impose a fundamental limit to the performance of a GaN-based HEMT.

In this letter, we present our results following the investigation of the nonequilibrium LO phonons in a biased GaN/AlN heterostructure based on first-order and second-order resonant Raman scatterings.

Our GaN/AlN heterostructure was grown using molecular beam epitaxy. A 200-nm-thick unintentionally doped GaN layer was grown on the top of a 3-μm-thick semi-insulating GaN layer, which was first deposited on the top of the 300 μm sapphire substrate. Subsequently, the GaN layer was capped by a 4-nm-thick AlN layer. High-density two-dimensional electrons were confined within the GaN layer next to the GaN/AlN interface.[13] Source and drain Ohmic contacts were formed by the evaporation of the gold film followed by annealing. The gate was measured to be 30 μm in length. At room temperature, the electron sheet concentration and mobility were measured to be 2.5×10^{13} cm^{-2} and 1200 cm^2/V s, respectively.

A Raman signal backward-scattered by the AlN side of the HEMT was collected using a two-stage cascaded monochromator at room temperature (295 K) with different biases applied between the source and the drain in the range of 0–36 V. The outgoing Raman signal was then measured using a photomultiplier tube after going through the monochromator. A coherent picosecond radiation with the output wavelength in the range of 369–385 nm, produced by frequency doubling mode-locked picosecond Ti:sapphire laser output in a 10-mm-thick beta barium borate crystal, was used as an incident beam. The width of each incident pulse was measured to be 3 ps. During each measurement, a typical average incident power of 30 mW was used. The incident beam was focused down to the HEMT with a beam radius of $\sim$150 μm. The lattice temperature of the HEMT under a fixed bias was deduced by fitting the photoluminescence spectral profiles on the low-energy side, generated by a picosecond coherent UV radiation, using Boltzmann distribution.[14] As a result, we obtained the bandgap $E_g(T)$ for the GaN channel at each fixed dc electric field. Using Ref. 15, we deduced the corresponding dc lattice temperature.

The temperatures of the LO phonons are determined to be

$$T_{1\mathrm{LO}} = \frac{\hbar\omega_{\mathrm{LO}}}{k_B \ln[(n^{(1)}+1)/n^{(1)}]}, \tag{1}$$

where $n^{(1)}$ is the phonon occupation number for the first-order Raman scattering.[7] The two peaks resolved in Fig. 1 correspond to the first-order and second-order Raman scatterings of the picosecond incident pulses by the LO phonons with their energies being $\hbar\omega_{\mathrm{LO}}\approx91.8$ meV in the GaN channel layer. At different electric fields or incident photon energies, the intensities for the first-order and second-order Stokes and anti-Stokes Raman scatterings are different (see Fig. 2). Each of the four Raman scattering processes is going through its own resonance at a specific electric field.

a)Electronic mail: yud2@lehigh.edu.

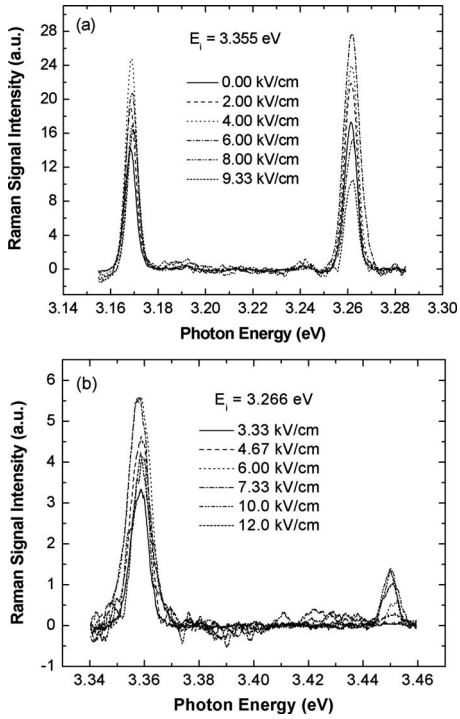

FIG. 1. Spectra of first-order and second-order (a) Stokes and (b) anti-Stokes Raman scatterings at different electric fields indicated. E_i is used to designate the photon energy of the incident beam.

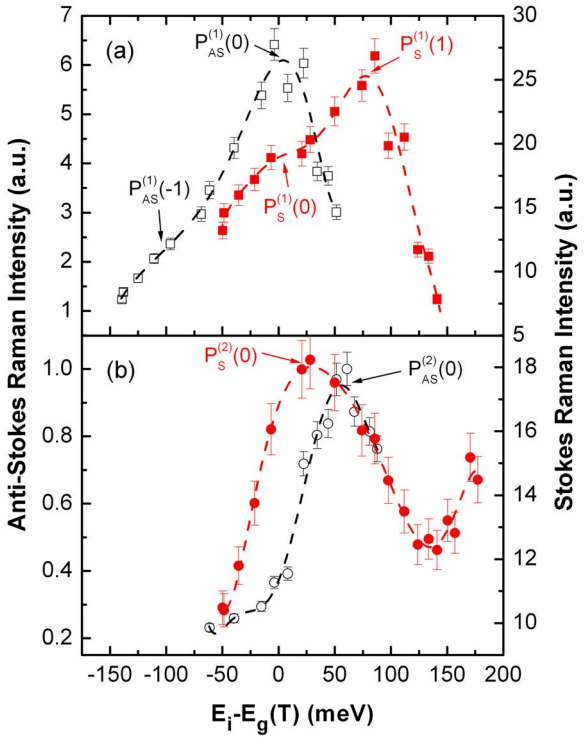

FIG. 2. (Color online) Dependences of (a) first-order and (b) second-order Raman scattering signal intensities deduced from Fig. 1 on the photon energy of the incident beam measured relative to the bandgap of GaN. Filled squares and filled circles, Stokes; open squares and open circles, anti-Stokes. All dashed curves correspond to fitting to data. The errors are indicated in the figures.

One can see from Fig. 2 that for the first-order Raman scattering there are two dominant peaks labeled as $P_{AS}^{(1)}(0)$ and $P_S^{(1)}(1)$ corresponding to the anti-Stokes and Stokes Raman scattering at E_i-$E_g \approx 3$ meV and E_i-$E_g \approx 80$ meV, respectively. According to Ref. 15, these two peaks correspond to the resonances for the incoming and outgoing photons to the bandgap of the GaN channel, respectively. A tail $P_{AS}^{(1)}(-1)$ and a shoulder $P_S^{(1)}(0)$ can be attributed to the anti-Stokes and Stokes Raman scatterings at E_i-$E_g \approx -96$ meV and E_i-$E_g \approx 0$ meV, respectively. They correspond to the resonances of the outgoing and incoming photon energies to the bandgap, respectively. The resonance for the incoming photons $P_S^{(1)}(0)$ is much weaker than that for the outgoing photons $P_S^{(1)}(1)$. For the resonance of the outgoing photons, free excitons are generated by the incoming photons, which further enhance the Raman signal intensities (i.e., a double resonance). For the first-order anti-Stokes Raman scattering, however, the resonance for the incoming photons $P_{AS}^{(1)}(0)$ is much stronger than that for the outgoing photons $P_{AS}^{(1)}(-1)$. Such behaviors are quite different from Ref. 16. In our heterostructure the generation of the electrons and their subsequent drift in a dc electric field have further enhanced $P_{AS}^{(1)}(0)$ and $P_S^{(1)}(1)$.

One can see from Fig. 2(b) that for the second-order Raman scattering, two resonant peaks labeled as $P_S^{(2)}(0)$ and $P_{AS}^{(2)}(0)$ are located at E_i-$E_g(T) \approx 27$ meV and E_i-$E_g(T) \approx 56$ meV, respectively. In our experiment, without applying a bias to the GaN/AlN heterostructure, we could not observe any second-order anti-Stokes Raman signal regardless of the detuning. After applying a relatively high electric field, the second-order anti-Stokes Raman peak becomes obvious. Moreover, the Raman signal can be significantly enhanced as the electric field is further increased (see Fig. 1). Such an enhancement caused by the increase in the electric field is an evidence of the presence of the hot phonons. For the second-order Raman scattering, two LO phonons must be absorbed or emitted simultaneously. The increase in the Raman signal intensity starting at E_i-$E_g(T) \approx 150$ meV in Fig. 2 could be caused by a resonant peak for the Stokes Raman scattering at E_i-$E_g(T) \approx 184$ meV (i.e., twice the LO phonon energy).

Using Eq. (1), we have determined the phonon temperatures from the first-order Raman scattering. For the incident photon energies of 3.355 and 3.266 eV, the phonon temperature increases at almost the same rate as the lattice temperature for the electric fields in the range of 0–5.33 kV/cm (see Fig. 3). Within such a range the increase in the electric field results in the increase in the lattice temperature, and therefore, the increase in phonon temperature. Above 5.33 kV/cm, however, the increase in the phonon temperature is much steeper than that in the lattice temperature (see Fig. 3). This implies that in such a range the increase in the electric field leads to the generation of additional LO phonons within 3 ps above those determined from the thermal equilibrium at the lattice temperature. Assuming that an electron is accelerated from zero kinetic energy to $\hbar\omega_{LO}$ under an electric field of E_{dc}, one can then estimate the duration of the acceleration to be 0.86 ps. This value is in the same order of magnitude as the decay time constant for the LO phonons.[5] Therefore, the LO phonons generated by the drifting electrons are excessively accumulated. Based on our experimental result (Fig. 3), the highest phonon temperature is determined to be 1290 K at the electric field of 11.3 kV/cm, which is higher than the lattice temperature by 583 K.

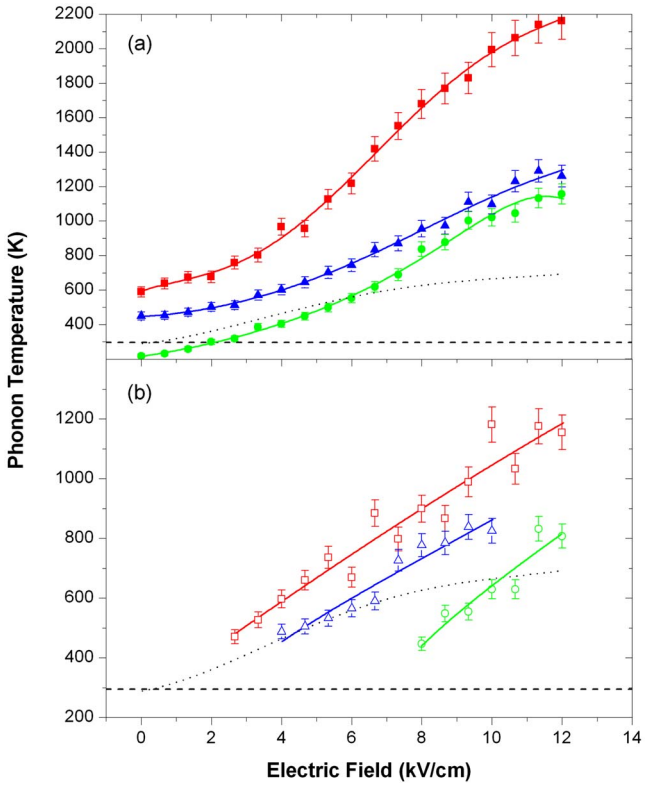

FIG. 3. (Color online) LO photon temperatures vs electric field, deduced from (a) first-order (filled symbols) and (b) second-order (open symbols) Raman scatterings, as a function of the electric field at three different sets of photon energies for the incident beam: 3.361 and 3.270 eV (filled and open squares), 3.355 and 3.266 eV (filled and open triangles), and 3.316 and 3.225 eV (filled and open circles). Solid curves, dotted curves, and horizontal dashed lines correspond to fitting to data, lattice temperatures, and room temperature (i.e., 295 K), respectively. The errors are indicated in the figures.

On the other hand, the phonon temperatures determined from the second-order Raman scattering are considerably lower [see Fig. 3(b)]. According to Ref. 17, the wave vectors of the two LO phonons participating in the second-order Raman scattering must obey a simple selection rule of $\vec{q}_1+\vec{q}_2=\vec{k}_L-\vec{k}_S$ due to conservation of momentum. Therefore, the LO phonons within the entire Brillouin zone participate in such a process. In such a case, the phonon temperature deduced from the second-order Raman scattering represents an average temperature for the LO phonons within the entire Brillouin zone. In contrast, for the first-order Raman scattering only the LO phonons with the proper values of the wave vectors participate in the process since $\vec{q}=\vec{k}_L-\vec{k}_S$. At a relatively low electric field, the phonon temperature $T_{2\mathrm{LO}}$ is about the same as the corresponding lattice temperature [see Fig. 3(b)]. As the electric field is increased, however, the phonon temperature becomes higher than the lattice temperature. However, it is increased at a rate much lower than that for the first-order Raman scattering (see Fig. 3). The highest phonon temperature is 839 K at the electric field of 9.33 kV/cm. In comparison, the phonon temperature determined from the first-order Raman scattering at the same electric field is 1110 K.

According to Fig. 3(b), it appears to us that the rates of the increases in the phonon temperatures are significantly less than those determined for the first-order Raman scattering. Since two LO phonons are simultaneously absorbed or emitted for the second-order Raman scattering, the temperature determined from the second-order Raman scattering represents an average value over the LO phonons within the entire Brillouin zone. This is the reason why the increases in the phonon temperatures as the incident photon energies are increased, determined for the second-order Raman scattering, should be much less. According to Fig. 3(b), the lowest electric field measured at which the second-order anti-Stokes Raman peak is observable is decreased as the photon energy is increased, which can be viewed as an evidence on the generation of the hot LO phonons by the picosecond incident pulses.

In conclusion, we have investigated the nonequilibrium LO phonons caused by the first-order Stokes and anti-Stokes resonant Raman scatterings in the presence of an electric field in a GaN/AlN heterostructure. By increasing the electric field to a relatively high value, the nonequilibrium LO phonons are generated by the electrons drifting in the electric field. The phonon temperatures deduced from the first-order Raman are much higher than the corresponding lattice temperatures whereas those deduced from the second-order Raman are considerably lower.

This work has been supported by the U.S. AFOSR.

[1] B. K. Ridley, Semicond. Sci. Technol. **4**, 1142 (1989).
[2] K. T. Tsen, D. K. Ferry, A. Botchkarev, B. Sverdlov, A. Salvador, and H. Morkoç, Appl. Phys. Lett. **71**, 1852 (1997).
[3] S. K. Tripathy, G. Xu, X. Mu, Y. J. Ding, K. Wang, Y. Cao, D. Jena, and J. B. Khurgin, Appl. Phys. Lett. **92**, 013513 (2008).
[4] B. K. Ridley, J. Phys.: Condens. Matter **8**, L511 (1996).
[5] K. T. Tsen, D. K. Ferry, A. Botchkarev, B. Sverdlov, A. Salvador, and H. Morkoç, Appl. Phys. Lett. **72**, 2132 (1998).
[6] A. Matulionis, J. Liberis, I. Matulioniene, M. Ramonas, L. F. Eastman, J. R. Shealy, V. Tilak, and A. Vertiatchikh, Phys. Rev. B **68**, 035338 (2003).
[7] K. T. Tsen, K. R. Wald, T. Ruf, P. Y. Yu, and H. Morkoç, Phys. Rev. Lett. **67**, 2557 (1991).
[8] B. K. Ridley, W. J. Schaff, and L. F. Eastman, J. Appl. Phys. **96**, 1499 (2004).
[9] C. H. Oxley, M. J. Uren, A. Coates, and D. G. Hayes, IEEE Trans. Electron Devices **53**, 565 (2006).
[10] M. Ramonas, A. Matulionis, J. Liberis, L. F. Eastman, X. Chen, and Y. J. Sun, Phys. Rev. B **71**, 075324 (2005).
[11] J. Khurgin, Y. J. Ding, and D. Jena, Appl. Phys. Lett. **91**, 252104 (2007).
[12] T. Palacios, A. Chakraborty, S. Heikman, S. Keller, S. P. DenBaars, and U. K. Mishra, IEEE Electron Device Lett. **27**, 13 (2006).
[13] Z. Wang, K. Reimann, M. Woerner, T. Elsaesser, D. Hofstetter, J. Hwang, W. J. Schaff, and L. F. Eastman, Phys. Rev. Lett. **94**, 037403 (2005).
[14] D. S. Kim and P. Y. Yu, Phys. Rev. B **43**, 4158 (1991).
[15] I. Vurgaftman and J. R. Meyer, J. Appl. Phys. **94**, 3675 (2003).
[16] J. Reydellet, P. Y. Yu, J. M. Besson, and M. Balkanski, in *Physics of Semiconductors 1978*, edited by B. L. H. Wilson (Institute of Physics, Bristol, UK, 1979), pp. 1271–1274.
[17] A. Garcia-Cristóbal, A. Cantarero, C. T. Giner, and M. Cardona, Phys. Rev. B **49**, 13430 (1994).